Rev.Adv.Mater.Sci. 13 (2006) 6-14

THE CHARACTERISTICS OF GRAIN REFINEMENT IN MATERIALS PROCESSED BY SEVERE PLASTIC DEFORMATION

Terence G. Langdon

Departments of Aerospace & Mechanical Engineering and Materials Science
University of Southern California, Los Angeles, CA 90089-1453, USA

Received: June 20, 2006

Abstract. Processing by severe plastic deformation (SPD) provides the opportunity to achieve remarkable grain refinement in bulk crystalline solids. Typically, materials processed by SPD have grain sizes in the submicrometer or nanometer range. Several different SPD processing techniques are now available but the procedure currently receiving the most attention is equal-channel angular pressing (ECAP). In processing by ECAP, it is possible to obtain detailed information on the nature of grain refinement from systematic experiments conducted on single crystals and polycrystalline samples. This paper describes the types of results obtained when ECAP is applied to single crystal and polycrystalline aluminum. It is shown that the experimental results are consistent with expectations based on analyses of the processing behavior. The results permit the development of a simple model describing grain refinement in ECAP.

1. INTRODUCTION

The grain size of polycrystalline materials plays a critical role in determining the mechanical behavior of the material. At low temperatures the strength increases with decreasing grain size through the Hall-Petch relationship [1,2] but at high temperatures, when diffusion becomes important, the material flows more rapidly when the grain size is reduced [3]. Thermo-mechanical processing is generally used in industrial operations to achieve a range of acceptable grain sizes for different applications but the smallest grain sizes attained in this way are typically of the order of a few micrometers.

Two different types of processing technique have been developed in attempts to achieve exceptionally small grain sizes in the submicrometer and nanometer range [4]. The first technique, known as the 'bottom-up' approach, assembles materials on a block-by-block basis from individual atoms or nanoparticles. Examples of these procedures include inert gas condensation [5], electrodeposition [6] and ball milling with subsequent consolidation [7]. However, a disadvantage of these methods is that they are generally limited to the production of exceptionally small samples suitable for use in applications such as micro-electronics and they are not amenable for use in large-scale structural applications. In addition, these samples invariably contain some contaminants and at least a low level of residual porosity. These problems may be avoided by adopting the alternative 'top-down' approach where relatively large bulk materials, already available with large grain sizes, are processed in specialized ways in order to introduce exceptional grain refinement. Generally, grain refinement is achieved through the imposition of severe plastic deformation (SPD) [8,9] and therefore through the introduction of a high density of dislocations such that the dislocations are able to subsequently re-arrange to form a network of grain or subgrain boundaries. Several different SPD processing techniques are now available including equal-channel angular pressing (ECAP) [10], high-pressure torsion (HPT) [11] and accumulative roll-bonding (ARB) [12]. However, most attention has been given to date to ECAP be-

Corresponding author: Terence G. Langdon, e-mail: langdon@usc.edu

cause the process can be established readily in any standard metallurgical laboratory and it is easily scaled up for the processing of relatively large billets [13].

This paper is concerned with the characteristics of grain refinement when pure metals or metallic alloys are processed by ECAP. This technique involves pressing a billet through a die with the billet constrained within a channel which is bent through an abrupt angle within the die. Although the principles of ECAP processing were first introduced approximately twenty-five years ago [14], it is only very recently that the ECAP procedure has been applied to the processing of single crystals. Nevertheless, pressing with single crystals provides an important advantage over the use of conventional polycrystalline samples because the crystals are easily rotated prior to pressing to provide different crystal orientations with respect to both the pressing direction and the theoretical shear plane. An example of the pressing of single crystals is described in the following section, the application of ECAP to polycrystalline samples is considered in section 3 and finally the experimental data are used to outline a simple model for grain refinement during the ECAP process.

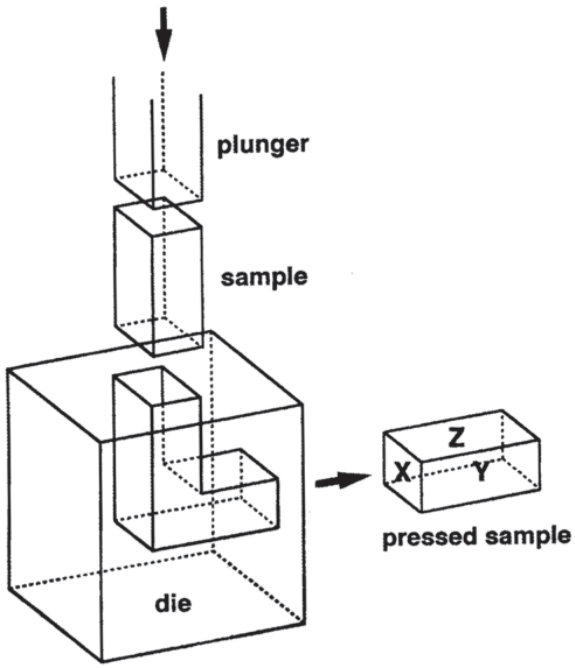

Fig. 1. The principle of ECAP showing the three orthogonal planes of sectioning [15].

2. PROCESSING OF SINGLE CRYSTALS BY ECAP

The principle of ECAP is depicted schematically in Fig. 1 [15]. The ECAP die contains a channel bent through a sharp angle and the sample is machined to fit within the channel and it is then pressed through the die using a plunger. Also shown in Fig. 1 are three orthogonal planes of sectioning designated the *X*, *Y* and *Z* planes.

The important characteristic of ECAP is that the sample emerges from the die without any change in the cross-sectional dimensions, thereby providing an opportunity for repetitive pressings through the die in order to attain very high strains. The strain imposed in ECAP is dependent upon two angles and these are the channel angle, Φ, which denotes the angle between the two parts of the channel and the angle, Ψ, at the outer arc of curvature where the two channels intersect: in Fig. 1, a die is shown with $\Phi = 90°$ and $\Psi = 0°$. In practice, it can be shown from first principles that the imposed strain in a single pass depends exclusively upon the values of the angles Φ and Ψ and the total strain is ~1 if the channel angle is $\Phi = 90°$ for any value of Ψ [16].

Several experiments have been conducted using single crystals of high-purity aluminum having different initial orientations [17-19]. In order to understand these orientations, Fig. 2 depicts a section through an ECAP die where the channel angle is $\Phi = 90°$, the outer arc of curvature is $\Psi = 0°$ and the sample, in the form of a single crystal, is pressed downwards in the vertical part of the channel [17]. Fig. 2 shows also the three orthogonal axes corresponding to the planes delineated in Fig. 1. Since $\Phi = 90°$ in Fig. 2, the theoretical shear plane lies at 45° to the *X* direction and shearing occurs as denoted by the arrows. For the crystal shown in Fig. 2, the [111] slip plane is oriented parallel to the theoretical shear plane, the <110> slip direction is parallel to the direction of shearing and the <112> direction lies along the *Y* axis. This orientation, where the theoretical shear plane and the [111] slip plane are coincident, is termed the 0° orientation. Experiments have been conducted using crystals in the 0° orientation [17] and in orientations where the crystal is rotated about the *Y* direction either in a counter-clockwise sense by 20° to give the -20°

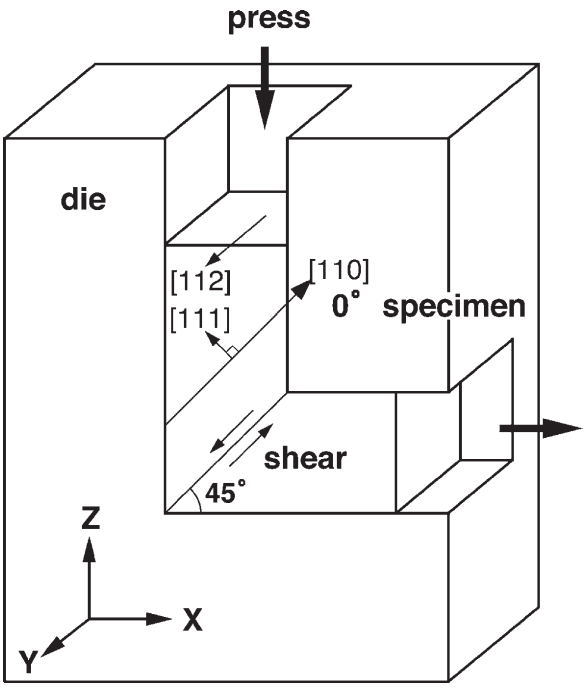

Fig. 2. Cross-section through an ECAP die showing the initial orientation for a single crystal: this is designated the 0° orientation [17].

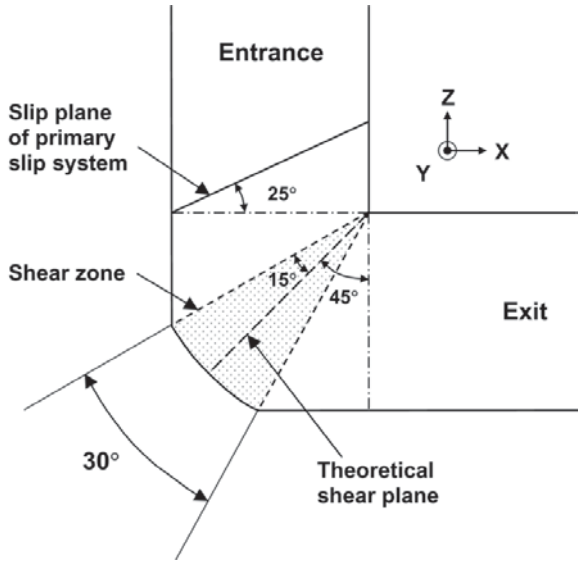

Fig. 3. The shape of the channel within the die used for the pressing of a single crystal: the arc of curvature of 30° introduces a shear zone when the sample passes through the die [19].

orientation [18] or in a clockwise sense by 20° to give the +20° orientation [19].

It is convenient to examine the results obtained when using single crystals orientated in the +20° orientation. This orientation is significant because the experiments were conducted using a die having a channel angle of $\Phi = 90°$ and an outer arc of curvature of $\Psi \approx 30°$ [19]. Fig. 3 illustrates the situation when using a die with $\Phi = 90°$ where there is an arc of curvature of 30° and the entrance to the die lies at the upper left. For this situation the shearing no longer takes place along a discrete and well-defined shear plane but instead there is a shear zone extending through an angular increment of ~30°. Thus, when the single crystal is initially oriented into the +20° orientation, it is apparent that the slip plane of the primary slip system lies along the line depicted in Fig. 3 and this is essentially coincident with the perimeter of the shear zone encountered during the pressing operation.

A single crystal was pressed through one pass and Fig. 4 shows the microstructure visible by transmission electron microscopy (TEM) on the *Y* plane in the vicinity of the central region of the crystal: the *X* and *Z* directions are parallel to the lower and side edges of the photomicrograph and the selected area electron diffraction (SAED) pattern was taken using a beam diameter of 12.3 μm [19]. The SAED pattern shows that the boundaries have low angles of misorientation and therefore the microstructure consists of a very well-defined array of elongated subgrains lying in the form of parallel bands and inclined at an angle of ~65° with the *X* axis. Measurements showed these subgrain bands have an average width of ~1.3 μm. The inclination at 65° to the *X* axis is a direct consequence of a rotation of the sample as it passes through the ECAP die, since it is apparent from Fig. 3 that this angle corresponds essentially to the orientation of the primary slip plane at the point of exit from the shear zone. Furthermore, close inspection showed that the longer axes of the subgrains lie parallel to the slip traces of the $(\bar{1}\,\bar{1}\,\bar{1})[\bar{1}10]$ slip system so that the elongated subgrains produced by ECAP in single crystals have their longer sides parallel to the primary slip plane. These results provide important information for the processing of polycrystalline samples by ECAP.

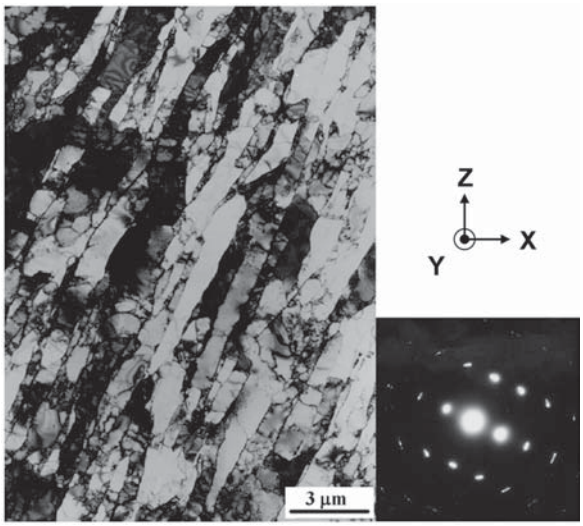

Fig. 4. Microstructure on the *Y* plane for an aluminum single crystal having a +20° orientation pressed through one pass [19].

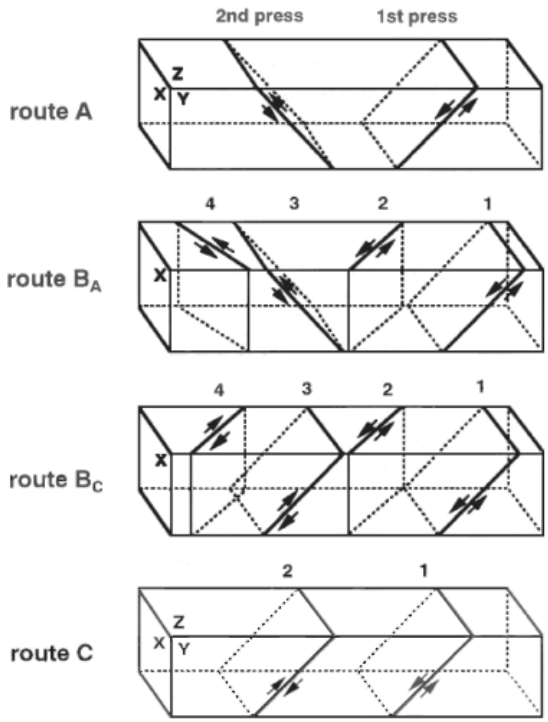

Fig. 5. The slip systems viewed on the *X*, *Y* and *Z* planes for consecutive passes using processing routes A, B_A, B_C, and C [22].

3. PROCESSING OF POLYCRYSTALLINE MATERIALS BY ECAP

3.1. Principles of processing through multiple passes

When a billet is pressed through an ECAP die, the cross-sectional area remains unchanged as illustrated in Fig. 1. Accordingly, it is feasible to press the same billet through multiple passes in order to attain very high strains. It was noted in early studies that different slip systems may be activated by simply rotating the billet about the longitudinal axis between consecutive passes [20]. At the present time, four major processing routes are in use in ECAP: these are route A where the sample is not rotated between passes, route B_A where the sample is rotated by 90° in alternate directions between each pass, route B_C where the sample is rotated by 90° in the same sense between passes and route C where the sample is rotated by 180° between passes [21].

In order to understand the significance of these different processing routes, it is necessary to consider the slip systems as depicted schematically in Fig. 5 where the *X*, *Y* and *Z* planes correspond to the planes defined earlier in Fig. 1 and the numbers 1 through 4 denote the active slip in different passes for each processing route [22]. Thus, route C is a simple processing route because the strain is restored after every two passes, whereas routes A and B_A are more complex because there is a cumulative build-up of strain in consecutive passes. In practice, route B_C is the optimum processing route because slip on the first and third passes, and also on the second and fourth passes, cancel to give a zero net strain after every four passes. Experiments show that, when using a die with $\Phi = 90°$, this processing route leads most expeditiously to a reasonably homogeneous and three-dimensional array of grains with boundaries having high angles of misorientation [23].

To understand the significance of these slip systems, it is instructive to examine the nature of the shearing patterns introduced during ECAP. Fig. 6 shows the slip traces on the *X*, *Y* and *Z* planes for 1 pass on the top line and for 2, 3 and 4 passes when using processing routes A, B_A, B_C and C with a die having a channel angle of 90° and with the samples rotated about the longitudinal axis [24]. Thus, for each plane of sectioning and each pos-

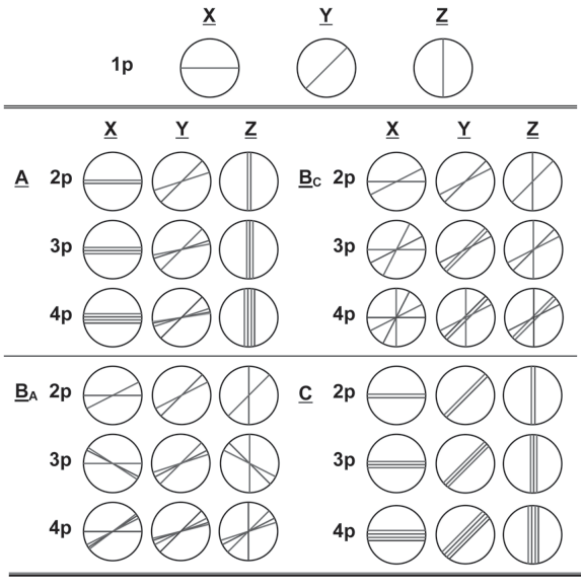

Fig. 6. The shearing patterns on the *X*, *Y* and *Z* planes for processing routes A, B_A, B_C and C: the top line shows the patterns after 1 pass and the other lines show the patterns after 2, 3, and 4 passes [24].

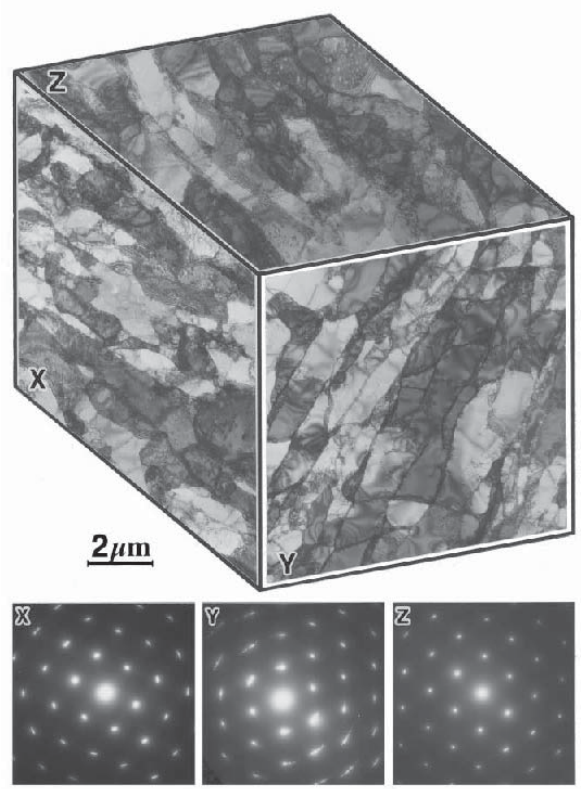

Fig. 7. Appearance of the microstructure of high-purity polycrystalline aluminum on the *X*, *Y,* and *Z* planes after one pass, together with the SAED patterns [25].

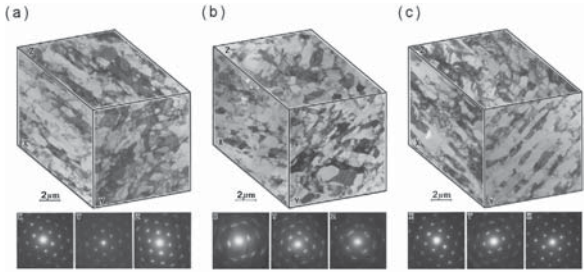

Fig. 8. Appearance of the microstructures of high-purity polycrystalline aluminum on the *X*, *Y,* and *Z* planes after two passes for (a) route A, (b) route B_C and (c) route C, together with the SAED patterns [25].

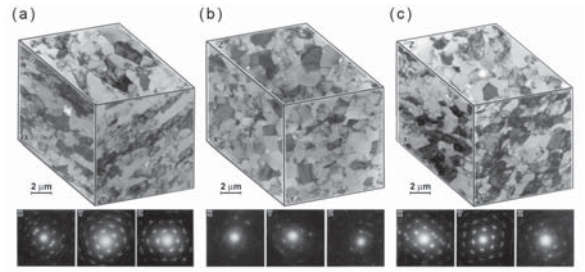

Fig. 9. Appearance of the microstructures of high-purity polycrystalline aluminum on the *X*, *Y,* and *Z* planes after four passes for (a) route A, (b) route B_C, and (c) route C, together with the SAED patterns [25].

sible processing route, Fig. 6 delineates the slip traces observed through consecutive passes. The important conclusion from Fig. 6 is that there is a large variation in the total angular spread of slip when viewed on the different planes. This angular spread includes a range of zero in route C where slip occurs repetitively on the same slip systems on all three planes and zero also in route A when viewed on the *X* or *Z* planes. By contrast, the angular range is fairly large in route B_C on all three planes of sectioning.

3.2. Application of this approach to the pressing of polycrystalline materials

The significance of these predicted slip traces may be examined by performing experiments and examining the slip on each orthogonal plane after different numbers of passes. This experiment was conducted using high purity aluminum with an initial grain size of ~1.0 mm and Figs. 7, 8, and 9 show the microstructures observed by TEM on the

X, *Y* and *Z* planes after a single pass, after 2 passes and after 4 passes, respectively: the planes are oriented with the *X* plane on the left, the *Y* plane on the right and the *Z* plane at the top, the photomicrographs after 2 and 4 passes relate to (a) route A, (b) route B_C and (c) route C and the SAED patterns shown below each cubic element denote the three planes of sectioning where the patterns were recorded using a beam diameter of 12.3 mm [25]. Inspection of the SAED patterns shows the boundaries have low angles of misorientation after 1 pass in Fig. 7 but the misorientation angles gradually increase and high angle boundaries are present after processing through 4 passes in route B_C.

The experimental results in Figs. 7-9 can be compared directly with the theoretical predictions in Fig. 6. First, for a single pass in Fig. 7, the microstructures on each plane consist of arrays of elongated subgrains defined by boundaries having low angles of misorientation and these subgrain arrays lie essentially horizontal when viewed on the *X* plane, at an angle of approximately 45° to the *X* axis when viewed on the *Y* plane and perpendicular to the direction of flow when viewed on the *Z* plane. Thus, the appearance of the substructure in Fig. 7 is directly consistent with the expectations documented in the top line of Fig. 6. Furthermore, the appearance of the polycrystalline sample after a single pass when viewed on the *Y* plane is consistent with the observation described earlier and shown in Fig. 4, also on the *Y* plane, for a single crystal pressed through 1 pass. An additional observation is that the average width of the subgrain arrays visible in Fig. 7 was measured as ~1.2-1.3 μm which is identical to the subgrain width observed in the single crystal after 1 pass as shown in Fig. 4. These results demonstrate the similarities between the microstructures generated when single crystals are processed by ECAP and in the processing of polycrystalline materials.

Fig. 8 is also consistent with the predictions of Fig. 6 for samples taken through 2 passes. This similarity is complex in routes A and B_C because of the development of slip through a range of angles but the similarity is clearly demonstrated when processing in route C because the illustrations in Fig. 6 predict the development of slip on a series of parallel planes lying oriented in an identical manner to the slip orientations after a single pass in Fig. 8c. Thus, for example, the subgrain bands visible on the *Y* plane in Fig. 8c are well-defined and they are clearly oriented at 45° to the *X* axis and therefore to the pressing direction.

There is a gradual evolution in the microstructure with subsequent passes through the die and this is evident in Fig. 9 where the sample processed through route B_C exhibits well-defined arrays of reasonably homogeneous and essentially equiaxed grains which are essentially identical in appearance on each of the three orthogonal planes. For this condition using route B_C, there is a reasonable fraction of high-angle boundaries and the average grain size was measured as ~1.2-1.3 μm. This average size is therefore consistent both with the width of the subgrain bands visible after a single pass in Fig. 7 and with the width of the subgrain bands visible in the single crystal in Fig. 4. These experiments lead to the conclusion, therefore, that the ultimate average grain size which is achieved after processing by ECAP is dictated by the width of the elongated subgrain bands formed in the initial pass. Detailed analysis has shown also that the grain sizes produced by ECAP processing are almost identical to the subgrain sizes reported from tests conducted under conventional cold-working operations such as compression or extrusion [26].

4. DISCUSSION

The results of these experiments, when combined with other experimental data on the evolution of homogeneity in ECAP [27], may be used to construct a simple model for grain refinement during the pressing operation.

With reference to the shearing patterns visible in Fig. 6, the first important question concerns the individual angular ranges of slip which are present on each orthogonal plane after each separate pass through the ECAP die. Assuming that the total angular range is represented by η, and using the detailed three-dimensional analysis available elsewhere for a die with a channel angle of $\Phi = 90°$ [24], Table 1 summarizes the predictions for the three different processing routes considered in Figs. 8 and 9 after 2, 3, and 4 passes. Thus, the angular range remains at 0° for all three orthogonal planes when using processing route C and it remains at 0° also on planes *X* and *Z* for route A. However, route B_C is the optimum processing condition and for this route there are angular ranges of 90°, 63°, and 63° on planes *X*, *Y* and *Z* after pressing through a total of 4 passes. This large angular range is clearly conducive to developing an array of equiaxed ultrafine grains separated by high-angle boundaries when processing by ECAP.

A simple model for grain refinement is illustrated schematically in Fig. 10 [27] where this model ac-

Table 1. Angular ranges of slip for different processing routes.

Processing route	Number of passes	Total angular range, η		
		X	*Y*	*Z*
A	2p	0°	27°	0°
	3p	0°	34°	0°
	4p	0°	37°	0°
B_C	2p	27°	18°	45°
	3p	63°	18°	63°
	4p	90°	63°	63°
C	2p	0°	0°	0°
	3p	0°	0°	0°
	4p	0°	0°	0°

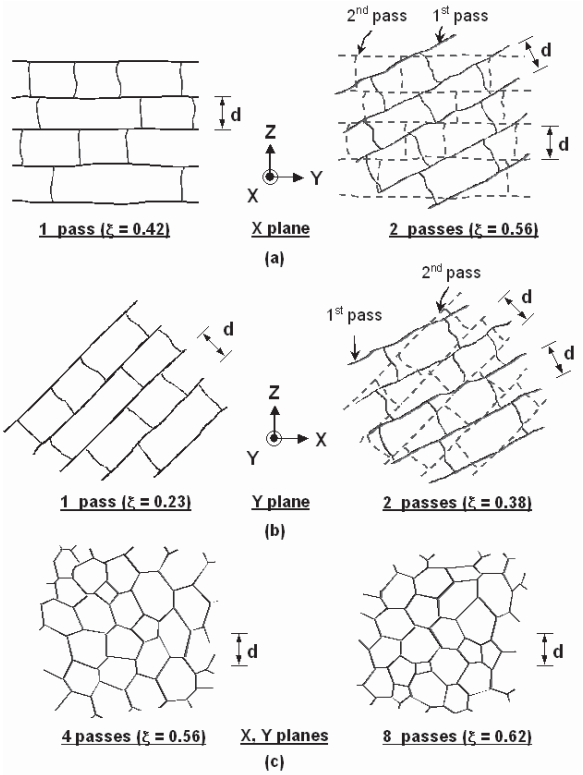

Fig. 10. A simple model for grain refinement in ECAP using processing route B_C [27].

counts for the behavior when pressing using route B_C and it is consistent with the experimental data for high-purity aluminum given in Figs. 7-9. The top row of Fig. 10 shows the microstructural development on the *X* plane after 1 pass (on the left) and 2 passes (on the right) and similar sketches are given in the second row for the appearance of the microstructure on the *Y* plane. Also, included in Fig. 10 are the experimental values for the fractions of boundaries having high angles of misorientation, ξ, using data taken from an earlier report for the pressing of high-purity aluminum [28]. Following the predictions from the top line for a single pass in Fig. 6, the model in Fig. 10 shows the bands of elongated subgrains lying horizontally and at approximately 45° to the pressing direction on the *X* and *Y* planes, respectively. For both of these conditions, the average width of the bands is given by *d*. After 2 passes, shown on the right in Figs. 10a and 10b, two sets of subgrain bands are superimposed following the angles of the slip traces illustrated in Fig. 6: these two sets of bands are designated 1st pass and 2nd pass, respectively, and again the new band introduced in the second pass has the same width of *d*.

As a consequence of microstructural evolution, the microstructures become similar on the *X*, *Y* and *Z* planes after 4 passes, as illustrated by the microstructures in Fig. 9b and by the illustration shown on the left in the bottom row of Fig. 10 where the final grain size is *d*. This microstructure remains similar with additional passes, as shown after 8 passes on the right in Fig. 10c. However, there is a gradual additional evolution of the microstructure because experiments show that the fraction of high-angle grain boundaries changes from $\xi \approx 0.56$ after 4 passes to $\xi \approx 0.62$ after 8 passes [28].

The model depicted in Fig. 10 provides a simple and realistic illustration of the microstructural changes occurring when high-purity aluminum is processed by ECAP using the optimum route B_C and an ECAP die with a channel angle of 90°. It is reasonable to anticipate there may be some minor differences in this basic model when other materi-

als are processed by ECAP: for example, it is well-established that the addition of magnesium to aluminum decreases the ultimate grain size such that more passes are needed to attain an ultimate equiaxed equilibrium grain size [29] and in materials such as copper there is a very low rate of recovery and microstructural evolution occurs exceptionally slowly with increasing numbers of passes [30]. Nevertheless, it is assumed that the simple model illustrated in Fig. 10 is consistent with microstructural development in a wide range of materials processed by ECAP.

5. SUMMARY AND CONCLUSIONS

1. The principles of grain refinement in equal-channel angular pressing (ECAP) are described using experimental data for high-purity aluminum in the form of both single crystals and polycrystalline materials.
2. There are experimental similarities between the microstructures observed in single crystals and in the polycrystalline samples when pressing with a die having a channel angle of 90°. Initially, the microstructure of the polycrystalline samples consists of bands of elongated subgrains after the first pass but these bands evolve with additional passes and ultimately, after 4 passes using route B_C where the samples are rotated by 90° in the same sense between each pass, there is a reasonably homogeneous and equiaxed array of grains separated by high-angle boundaries.
3. It is shown that the experimental results are consistent with the expectations from the theoretical shearing patterns. It is concluded that route B_C is the optimum processing route because it incorporates slip over the largest angular range.
4. The results are used to describe a simple model for grain refinement in ECAP.

ACKNOWLEDGEMENT

This work was supported by the U.S. Army Research Office under Grant No. W911NF-05-1-0046.

REFERENCES

[1] E.O. Hall // *Proc. Roy. Soc*. **B 64** (1951) 747.
[2] N.J. Petch // *J. Iron Steel Inst.* **174** (1953) 25.
[3] T.G. Langdon // *Mater. Sci. Eng.* **A166** (1993) 67.
[4] Y.T. Zhu, T.C. Lowe and T.G. Langdon // *Scripta Mater.* **51** (2004) 825.
[5] H. Gleiter // *Prog. Mater. Sci.* **33** (1989) 323.
[6] U. Erb, A.M. El-Sherik, G. Palumbo and K.T. Aust // *Nanostruct. Mater.* **2** (1993) 383.
[7] C.C. Koch and Y.S. Cho // *Nanostruct. Mater.* **1** (1992) 207.
[8] R.Z. Valiev, R.K. Islamgaliev and I.V. Alexandrov // *Prog. Mater. Sci.* **45** (2000) 103.
[9] R.Z. Valiev, Y. Estrin, Z. Horita, T.G. Langdon, M.J. Zehetbauer and Y.T. Zhu // *JOM* **58** (4) (2006) 33.
[10] R.Z. Valiev and T.G. Langdon // *Prog. Mater. Sci.* **51** (2006) 881.
[11] A.P. Zhilyaev, G.V. Nurislamova, B.-K. Kim, M.D. Baró, J.A. Szpunar and T.G. Langdon // *Acta Mater.* **51** (2003) 753.
[12] Y. Saito, H. Utsunomiya, N. Tsuji and T. Sakai // *Acta Mater.* **47** (1999) 579.
[13] Z. Horita, T. Fujinami and T.G. Langdon // *Mater. Sci. Eng.* **A318** (2001) 34.
[14] V.M. Segal, V.I. Reznikov, A.E. Drobyshevskiy and V.I. Kopylov // *Russian Metall.* **1** (1981) 99.
[15] P.B. Berbon, M. Furukawa, Z. Horita, M. Nemoto and T.G. Langdon // *Metall. Mater. Trans.* **30A** (1999) 1989.
[16] Y. Iwahashi, J. Wang, Z. Horita, M. Nemoto and T.G. Langdon // *Scripta Mater.* **35** (1996) 143.
[17] Y. Fukuda, K. Oh-ishi, M. Furukawa, Z. Horita and T.G. Langdon //*Acta Mater.* **52** (2004) 1387.
[18] M. Furukawa, Y. Kawasaki, Y. Miyahara, Z. Horita and T.G. Langdon // *Mater. Sci. Eng.* **A410-411** (2005) 194.
[19] Y. Fukuda, K. Oh-ishi, M. Furukawa, Z. Horita and T.G. Langdon // *Mater. Sci. Eng.* **A420** (2006) 79.
[20] V.M. Segal // *Mater. Sci. Eng.* **A197** (1995) 157.
[21] M. Furukawa, Y. Iwahashi, Z. Horita, M. Nemoto and T.G. Langdon // *Mater. Sci. Eng.* **A257** (1998) 328.
[22] M. Nemoto, M. Furukawa, Z. Horita and T.G. Langdon // *Metals Mater.* **4** (1998) 1181.
[23] K. Oh-ishi, Z. Horita, M. Furukawa, M. Nemoto and T.G. Langdon // *Metall. Mater. Trans.* **29A** (1998) 2011.
[24] M. Furukawa, Z. Horita and T.G. Langdon // *Mater. Sci. Eng.* **A332** (2002) 97.
[25] Y. Iwahashi, Z. Horita, M. Nemoto and T.G. Langdon // *Acta Mater.* **46** (1998) 3317.

[26] S.L. Semiatin, P.B. Berbon and T.G. Langdon // *Scripta Mater.* **44** (2001) 135.
[27] C. Xu, M. Furukawa, Z. Horita and T.G. Langdon // *Mater. Sci. Eng.* **A398** (2005) 66.
[28] S.D. Terhune, D.L. Swisher, K. Oh-ishi, Z. Horita, T.G. Langdon and T.R. McNelley // *Metall. Mater. Trans.* **33A** (2002) 2173.
[29] Y. Iwahashi, Z. Horita, M. Nemoto and T.G. Langdon // *Metall. Mater. Trans.* **29A** (1998) 2503.
[30] S. Komura, Z. Horita, M. Nemoto and T.G. Langdon // *J. Mater. Res.* **14** (1999) 4044.